Biochimica et Biophysica Acta 1828 (2013) 2513–2523

Contents lists available at ScienceDirect

Biochimica et Biophysica Acta

journal homepage: www.elsevier.com/locate/bbamem

How does acyl chain length affect thermotropic phase behavior of saturated diacylphosphatidylcholine–cholesterol binary bilayers?

Nobutake Tamai [a], Takuya Izumikawa [b], Suguru Fukui [b], Maiko Uemura [b], Masaki Goto [a], Hitoshi Matsuki [a,*], Shoji Kaneshina [a]

[a] Department of Life System, Institute of Technology and Science, The University of Tokushima, 2-1 Minamijosanjima-cho, Tokushima 770-8506, Japan
[b] Department of Biological Science and Technology, Faculty of Engineering, The University of Tokushima, 2-1 Minamijosanjima-cho, Tokushima 770-8506, Japan

ARTICLE INFO

Article history:
Received 30 November 2012
Received in revised form 31 May 2013
Accepted 11 June 2013
Available online 18 June 2013

Keywords:
Cholesterol
Diacylphosphatidylcholine
Peritectic point
Phase diagram
Lateral phase separation
Superlattice

ABSTRACT

Thermotropic phase behavior of diacylphosphatidylcholine (C*n*PC)–cholesterol binary bilayers (n = 14–16) was examined by fluorescence spectroscopy using 6-propionyl-2-(dimethylamino)naphthalene (Prodan) and differential scanning calorimetry. The former technique can detect structural changes of the bilayer in response to the changes in polarity around Prodan molecules partitioned in a relatively hydrophilic region of the bilayer, while the latter is sensitive to the conformational changes of the acyl chains. On the basis of the data from both techniques, we propose possible temperature T–cholesterol composition X_{ch} phase diagrams for these binary bilayers. A notable feature of our phase diagrams, including our previous results for diheptadecanoylphosphatidylcholine (C17PC) and distearoylphosphatidylcholine (C18PC), is that there is a peritectic-like point around X_{ch} = 0.15, which can be interpreted as indicating the formation of a 1:6-complex of cholesterol and C*n*PCs within the binary bilayer irrespective of the acyl chain length. We could give a reasonable explanation for such complex formation using the modified superlattice view. Our results also showed that the X_{ch} value of the abolition of the main transition is almost constant for n = 14–17 (ca. 0.33), while it increases to ca. 0.50 for n = 18. By contrast, a biphasic n-dependence of X_{ch} was observed for the abolition of the pretransition, suggesting that there are at least two antagonistic n-dependent factors. We speculate that this could be explained by the enhancement of the van der Waals interaction with increases in n and the weakening of the repulsion between the neighboring headgroups with decreases in n.

1. Introduction

Artificial phospholipid bilayer membranes composed of a single kind of phospholipid (i.e., pure phospholipid bilayer membranes), have long been used as models of biomembranes for better understanding the structure and physicochemical properties of cell membranes. Dipalmitoylphosphatidylcholine (C16PC) is one of the most frequently used phospholipids in model membrane studies, and it is well known for the C16PC bilayer [1,2] that a pretransition, or the transition from a lamellar gel ($L_{\beta'}$) phase to a ripple gel ($P_{\beta'}$), and a main transition, or the transition from the $P_{\beta'}$ phase to a liquid crystalline (L_{α}), take place at ca. 34 °C and ca. 42 °C under atmospheric pressure, respectively. It has also been clarified that both transitions take place at lower temperatures in bilayers of its homologues with shorter acyl chains [1,2], such as dipentadecanoylphosphatidylcholine (C15PC) and dimyristoylphosphatidylcholine (C14PC). On the other hand, as a recent trend in the model membrane studies, increasing use has been made of multi-component phospholipid bilayers containing cholesterol (Chol) because of the new model of the cell membrane proposed by Simons and Ikonen [3]. According to this model, the structure of the cell membrane is essentially heterogeneous and there exist microdomains, generally called lipid rafts, composed of specific kinds of phospholipids and Chol, which are thought to be involved in various cellular processes, such as protein sorting [3] and signal transduction [4]. In fact, it has been confirmed by direct observation with various kinds of visualization techniques that such domains are really formed in three-component model systems [5–7].

The effect of Chol on the structure and properties of phospholipid membranes began to be investigated long before the concept of the lipid raft was proposed [8]. Early studies revealed several key features: for example, Chol decreases the membrane fluidity in the L_{α} phase, whereas it conversely increases the fluidity in the gel phase [9]. It is also known that the orientational order of the phospholipid hydrocarbon chains is enhanced by the presence of Chol above the main-transition temperature [10]. These features can be interpreted to mean that Chol induces an intermediate state between the gel and the L_{α} states. Although the effects of Chol on the bilayer phase structure have been also intensely studied from the viewpoint of a temperature (T)–Chol composition (X_{ch}) phase diagram, unfortunately,

* Corresponding author at: Department of Life System, Institute of Technology and Science, The University of Tokushima, 2-1 Minamijosanjima-cho, Tokushima 770-8506, Japan. Tel.: +81 88 656 7513; fax: +81 88 655 3162.
E-mail address: matsuki@bio.tokushima-u.ac.jp (H. Matsuki).

0005-2736/$ – see front matter © 2013 Elsevier B.V. All rights reserved.
http://dx.doi.org/10.1016/j.bbamem.2013.06.008

most of the early studies [11,12] did not lead to complete elucidation of the phase behavior of the binary bilayers. A major reason for this is that the bilayer phase transitions tend to be obscured with increasing Chol content in the binary bilayer.

A breakthrough was achieved by Ipsen et al. [13], who determined the phase boundaries for the C16PC–Chol binary bilayer by theoretical calculations based on a thermodynamic and a simple microscopic model. The phase diagram they presented provided a number of significant features of the phase behavior of the Chol-containing binary bilayer. For example, they defined the phase state occurring in the higher Chol concentration region as a third phase that was distinguished from solid ordered (S_o) phase and liquid disordered (L_d) phase, and named it liquid ordered phase (i.e., L_o phase) considering that the new phase could be characterized by high conformational order of the acyl chains and rapid lateral diffusion. They also revealed that there is a two-phase region above the main-transition temperature due to the miscibility gap between the L_d and L_o phases. A few years later, ^{2}H NMR study by Vist and Davis [14] demonstrated that the experimental phase diagram for the perdeuterated C16PC–Chol binary bilayer was qualitatively similar to the theoretical phase diagram given by Ipsen et al. [13]. This qualitative agreement between the theoretical and the experimental phase diagrams of the C16PC–Chol binary bilayer strongly supported the validity of the theoretical consideration on the phase behavior of the Chol-containing binary bilayer and enhanced the reliability of the experimental phase diagram. Thereafter, phase diagrams with similar topology were reported for other kinds of phospholipid–Chol binary bilayers [15,16].

Now there still remain issues to be solved to completely elucidate the phase behavior of the Chol-containing binary bilayers. First, the phase diagrams by Ipsen et al. [13] and by Vist and Davis [14] have no indication about the pretransition. Second, it has not been clarified sufficiently how the chemical structure of the host phospholipid molecule affects the phase behavior of Chol-containing binary bilayers. McElhaney's group has systematically studied the Chol effect on the thermotropic bilayer phase behavior of various kinds of phospholipids using high-sensitivity differential scanning calorimetry (DSC) and Fourier transform infrared spectroscopy (FT-IR) in detail [17–20]. However, even they did not demonstrate how the feature of the phase diagram and the topology of the phase boundaries change with variations in the chemical structure of constituent phospholipids. As far as we know, only the study by Huang et al. [21] has addressed this issue, where the phase behavior of C*n*PC–Chol binary bilayers ($n = 16$, 18, and 20) has been investigated by means of solid-state NMR and high-sensitivity DSC. In a recent review by Marsh [22], the T–X_{ch} phase diagrams that have so far been reported for binary bilayers of various lipids with Chol have been collected together to compare and contrast those obtained by different experimental methods. As is evident from this review, systematic studies are still required to establish the phase diagrams of Chol-containing binary bilayers of various kinds of phospholipids.

In our previous papers [23,24], we reported the T–X_{ch} phase diagrams of the distearoylphosphatidylcholine (C18PC)– and the diheptadecanoylphosphatidylcholine (C17PC)–Chol binary bilayers, and also gave a new explanation for the X_{ch}-dependent phase behavior of those binary bilayers by applying the so-called *superlattice view*, proposed by Somerharju et al. [25]. In this study, we investigated the binary bilayers of C14PC–, C15PC– and C16PC–Chol using the same experimental techniques as used in our previous studies, namely DSC and fluorescence spectroscopy using 6-propionyl-2-(dimethylamino) naphthalene (Prodan) as a probe, to construct the T–X_{ch} phase diagrams. DSC is highly sensitive to energetic thermotropic events like conformational changes of the acyl chains of phospholipid molecules. Prodan is known as a polarity-sensitive membrane probe, and its emission spectrum varies sensitively in response to the change in polarity of the microenvironment around it [26–30]. Therefore, the combination of the two complementary techniques allows us to examine the phase behavior of those binary bilayers from different aspects. In addition, we applied the superlattice view based on the hexagonal lattice to the interpretation of the phase diagrams constructed to discuss the effect of the variation in the acyl chain length n of the host C*n*PC molecule on the phase behavior of the C*n*PC–Chol binary bilayers.

2. Materials and methods

Synthetic phosphatidylcholines, C14PC (1,2-dimyristoyl-*sn*-glycero-3-phosphocholine), C15PC (1,2-diheptadecanoyl-*sn*-glycero-3-phosphocholine) and C16PC (1,2-dipalmitoyl-*sn*-glycero-3-phosphocholine) were purchased from Avanti Polar Lipids (Alabaster, AL) and Chol (5-cholesten-3β-ol) was from Sigma-Aldrich Co. (St. Louis, MO). The fluorescent probe of Prodan (6-propionyl-2-(dimethylamino) naphthalene) was purchased from Molecular Probes Inc. (Eugene, OR). All the materials were used without further purification. Water used for preparing sample solutions was distilled twice from dilute alkaline permanganate solution. For each C*n*PC, multilamellar vesicle (MLV) dispersions with different Chol compositions were prepared by the following procedure. As a first step, an almost constant amount of phospholipid powder was taken into each of about 35 test tubes with a screw cap and weighed precisely. Immediately after that, stock solutions of Chol/chloroform (and Prodan/ethanol for fluorescence measurements) were prepared in Erlenmeyer flasks with a glass stopper. An appropriate volume of the stock solutions was added using a Gilson Pipetman to each test tube containing the weighed phospholipid powder. The weights of the added stock solutions were also determined. These operations were finished within one day without fail. All the solutions of C*n*PC/Chol/chloroform (or C*n*PC/Chol/Prodan/chloroform/ethanol for fluorescence measurements) thus prepared were stored in a refrigerator until used to prepare an aqueous dispersion of MLV a week (or a few days) before measurements were performed. Finally, we obtained a homogeneously translucent MLV dispersion by the following procedure: the solvent was removed completely in vacuum after the solution was transferred to an egg-plant shaped flask, and the resulting dry thin film of the lipid was dispersed by adding an appropriate amount of distilled water and by vortexing and sonication (a few minutes) at a temperature a few degrees higher than the main-transition temperature of each C*n*PC bilayer. The concentrations of C*n*PC and Prodan were fixed at 1 mmol kg^{-1} and 2 μmol kg^{-1} (i.e., molar ratio of C*n*PC to Prodan is 500:1), respectively [28]. The Chol composition in the bilayer was varied from 0 to 0.50 in mole fraction. Here, X_{ch} is defined using the molalities of Chol (m_{ch}) and C*n*PC (m_{PC}) as

$$X_{ch} = m_{ch}/(m_{ch} + m_{PC}) \quad (1)$$

The accuracy of the X_{ch} value was confirmed using commercially available assay kits for phospholipid (Phospholipid-C Test Wako, Wako Pure Chemical Industries, Ltd., Osaka) and Chol (Cholesterol-E Test Wako, Wako Pure Chemical Industries, Ltd., Osaka) for several sample dispersions.

The fluorescence measurements were performed using an F-3010 fluorescence spectrophotometer (Hitachi High-Technology Corp., Tokyo) at constant temperatures ranging from 30 to ca. 75 °C. The temperature was controlled within an accuracy of 0.1 °C by circulating thermostated water from a temperature-regulated water bath. The excitation wavelength was 361 nm and the emission spectra were recorded in the range of 400–600 nm.

DSC measurements were carried out using a high-sensitivity differential scanning calorimeter MCS (MicroCal, Northampton, MA). The heating rate was 0.33 °C min^{-1} and the temperature range was from ca. 10 to ca. 80 °C. The temperatures and enthalpy changes associated with the phase transitions were determined from endothermic peaks in the DSC thermograms by use of data-analyzing software ORIGIN supplied by MicroCal.

3. Results and discussion

3.1. Prodan fluorescence measurements

Fig. 1(a) shows the Prodan fluorescence spectra obtained for the pure C16PC bilayer at different temperatures ranging from 20 to 55 °C. A unique local emission maximum was observed in every spectrum in the wavelength range of 400–600 nm, and the wavelength at the maximum emission (λ_{max}) shifted toward higher wavelength region with increasing temperature. Similar behavior was observed for the pure C15PC and the pure C14PC bilayers. It has been confirmed for the bilayer membranes of various kinds of PCs [28,31] that the λ_{max} value changes from ca. 440 nm to a slightly higher wavelength at the pretransition (i.e., L_{β}'/P_{β}' transition) and further increases up to ca. 490 nm at the main transition (i.e., P_{β}'/L_{α} transition). Fig. 1(b)–(d) shows the Prodan fluorescence spectra obtained for the C16PC–Chol binary bilayers with different Chol compositions (X_{ch} = 0.08, 0.26 and 0.39) in the temperature range of 20–80 °C, respectively. Although the lineshapes of a series of the Prodan fluorescence spectra for the binary bilayers were somewhat different from those of the spectra for the pure C16PC bilayer, the λ_{max} shift from 440 nm to 490 nm with increasing temperature was observed for all the C16PC–Chol binary bilayers except for the one at X_{ch} = 0.39. This suggests that the λ_{max} value and the fluorescence intensities at 440 and 490 nm are available for pursuing the changes of the bilayer phase states with temperature also for the Chol-containing binary bilayers.

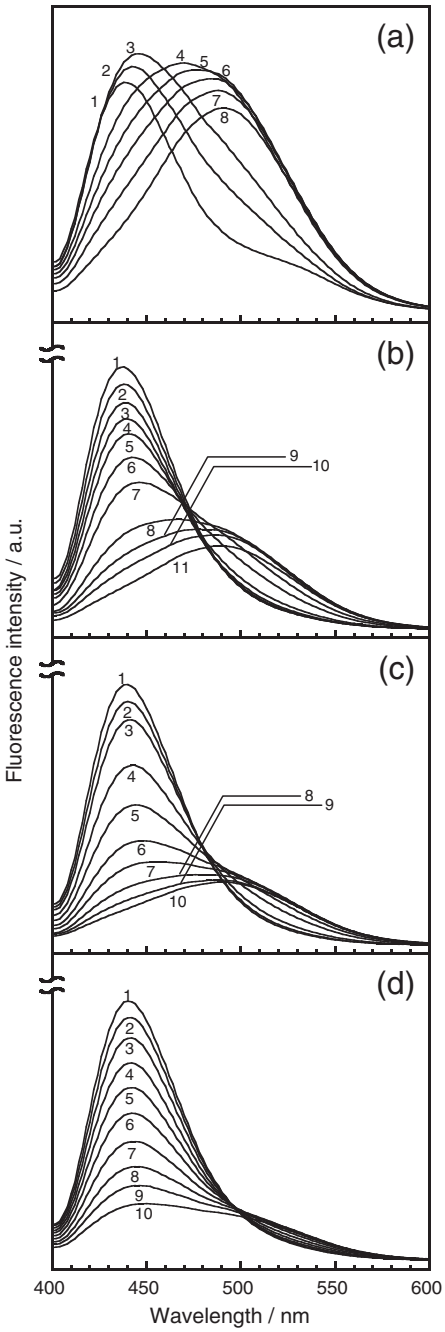

Fig. 1. Emission spectra of Prodan obtained at different temperatures for C16PC–cholesterol binary bilayer membranes at various cholesterol compositions (X_{ch}): (a) X_{ch} = 0, (b) 0.08, (c) 0.26 and (d) 0.39. The temperatures are represented by numbering each spectra as follows: (a) (1) 27.9 °C, (2) 33.9 °C, (3) 39.9 °C, (4) 40.9 °C, (5) 41.9 °C, (6) 43.9 °C, (7) 47.9 °C, and (8) 54.9 °C; (b) (1) 20.0 °C, (2) 24.0 °C, (3) 28.9 °C, (4) 33.9 °C, (5) 38.9 °C, (6) 39.9 °C, (7) 41.0 °C, (8) 45.9 °C, (9) 49.9 °C, (10) 53.9 °C, and (11) 59.9 °C; (c) (1) 29.9 °C, (2) 36.0 °C, (3) 41.0 °C, (4) 46.9 °C, (5) 51.9 °C, (6) 58.0 °C, (7) 62.9 °C, (8) 68.9 °C, (9) 74.0 °C, and (10) 79.9 °C; (d) (1) 30.0 °C, (2) 35.0 °C, (3) 40.0 °C, (4) 45.0 °C, (5) 49.9 °C, (6) 54.9 °C, (7) 60.0 °C, (8) 65.1 °C, (9) 69.9 °C, and (10) 74.9 °C.

Fig. 2 shows the temperature dependence of λ_{max} and the ratio of the fluorescence intensity at 440 nm to that at 490 nm (F_{440}/F_{490}) for the pure C16PC, C15PC and C14PC bilayers. With increasing temperature, the λ_{max} value increased slightly at the pretransition temperature (ca. 14 °C for C14PC, ca. 24 °C for C15PC and ca. 34 °C for C16PC [1,2]), and further increased steeply at the main-transition temperature (ca. 24 °C for C14PC, ca. 35 °C for C15PC and ca. 42 °C for C16PC [1,2]). In correspondence to the variation in λ_{max} with temperature, stepwise decreases in the ratio of F_{440}/F_{490} were observed at almost the same temperatures for each bilayer. For the C16PC and the C15PC bilayers, we defined the following two criteria

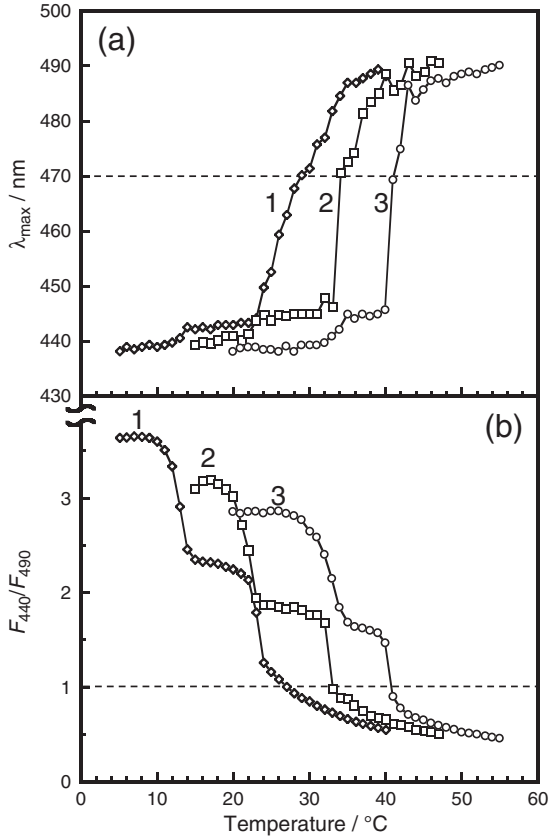

Fig. 2. Temperature dependence of (a) wavelength at the maximum emission (λ_{max}) and (b) ratio of the intensity at 440 nm (F_{440}) to that at 490 nm (F_{490}), i.e., F_{440}/F_{490}, for pure bilayer membranes of (1) C14PC, (2) C15PC and (3) C16PC. The dotted line in each panel indicates the criteria to determine the main-transition temperature (see text for details).

to determine the main-transition temperature on the basis of these temperature-dependence curves by taking into account that λ_{max} jumps up to 470 nm and simultaneously F_{490} becomes greater than F_{440}: one is $\lambda_{max} = 470$ nm and the other is $F_{440}/F_{490} = 1$. That is, the main-transition temperature was determined as the average of both temperatures at which the λ_{max} value exceeds 470 nm and at which the ratio F_{440}/F_{490} reduces to be less than 1. On the other hand, these criteria were not applicable to the results for the C14PC bilayer, because the variations of λ_{max} and F_{440}/F_{490} at the main transition were somewhat moderate compared to those for the other kinds of C*n*PC bilayers, and consequently these criteria provided slightly higher main-transition temperatures (ca. 27 °C). Then, we determined the main-transition temperature for a series of C14PC–Chol binary bilayers with different X_{ch} first by applying the same criteria and subsequently by correcting the temperature gap (i.e., ca. 3 °C). We have confirmed that this correction has no crucial effect on the thermodynamic features of the T–X_{ch} phase diagram.

Fig. 3(a)–(f) shows the temperature dependence of λ_{max} and F_{440}/F_{490} for the C14PC– ((a) and (b)), the C15PC– ((c) and (d)) and the C16PC–Chol ((e) and (f)) binary bilayers with different X_{ch}. At $X_{ch} = 0.01$, both temperature-dependence curves of λ_{max} and F_{440}/F_{490} for each binary bilayer were not significantly different from those for each pure bilayer, respectively. At $X_{ch} = 0.05$, however, the abrupt decrease in F_{440}/F_{490} in the lower temperature region was not seen and correspondingly no slight increase in λ_{max} in the same temperature region was observed for all the binary bilayers. This indicates that the pretransition of each bilayer is abolished by the incorporation of Chol corresponding to the X_{ch} of ca. 0.05. A further increase in X_{ch} gave rise to a noticeable influence on the temperature-dependence curves of λ_{max} and F_{440}/F_{490} for all the binary bilayers. The steep λ_{max} shift from ca. 440 nm to ca. 490 nm changed into a gradual increase, which took place in a finite temperature range, and the temperature range became wider with increasing X_{ch}. The decrease in F_{440}/F_{490} with temperature also became progressively gentle with increasing X_{ch}. This suggests that the conversion from an ordered state into a disordered state completes through some process over a finite temperature range. Therefore, we determined the lower and the higher limits of the temperature range from the break point and by using the criteria defined above, respectively, and regarded them as the onset and the completion point of the conversion, respectively. Finally, we could not observe the λ_{max} shift to ca. 490 nm and also the decrease of F_{440}/F_{490} below 1 within the temperature range in this study (up to ca. 80 °C) for each binary bilayer at $X_{ch} > 0.40$ (data not shown), suggesting that the binary bilayer no longer exhibits the conversion from the ordered state to the disordered state at that higher Chol composition.

3.2. DSC measurements

Fig. 4 shows the DSC thermograms for the pure C16PC bilayer and for the C16PC–Chol binary bilayers with different X_{ch}. For the pure bilayer, two endothermic peaks were observed at 34.5 °C and 41.6 °C, indicating that the bilayer underwent the pretransition and the main transition at those temperatures, respectively [1,2]. The endothermic peak of the pretransition became smaller with increasing X_{ch} and eventually undetectable above $X_{ch} = 0.08$. Similar behavior was observed for the C15PC– and the C14PC–Chol binary bilayers, but the X_{ch} value at which the pretransition peak disappeared was slightly different from that for the C16PC–Chol binary bilayer: $X_{ch} = 0.06$ for the C15PC– and the C14PC–Chol binary bilayers. As for the main transition, the endothermic peak gradually increased in width but steeply decreased in height as X_{ch} increased, and eventually, it became smaller as a whole with increasing X_{ch}. As seen from the inset of Fig. 4, at $X_{ch} = 0.07$ an obviously asymmetric peak was observed, which indicates that the endothermic peak of the main transition is composed of at least two component peaks with different heights and widths. At $X_{ch} = 0.14$ the peak heights of the two components became almost comparable,

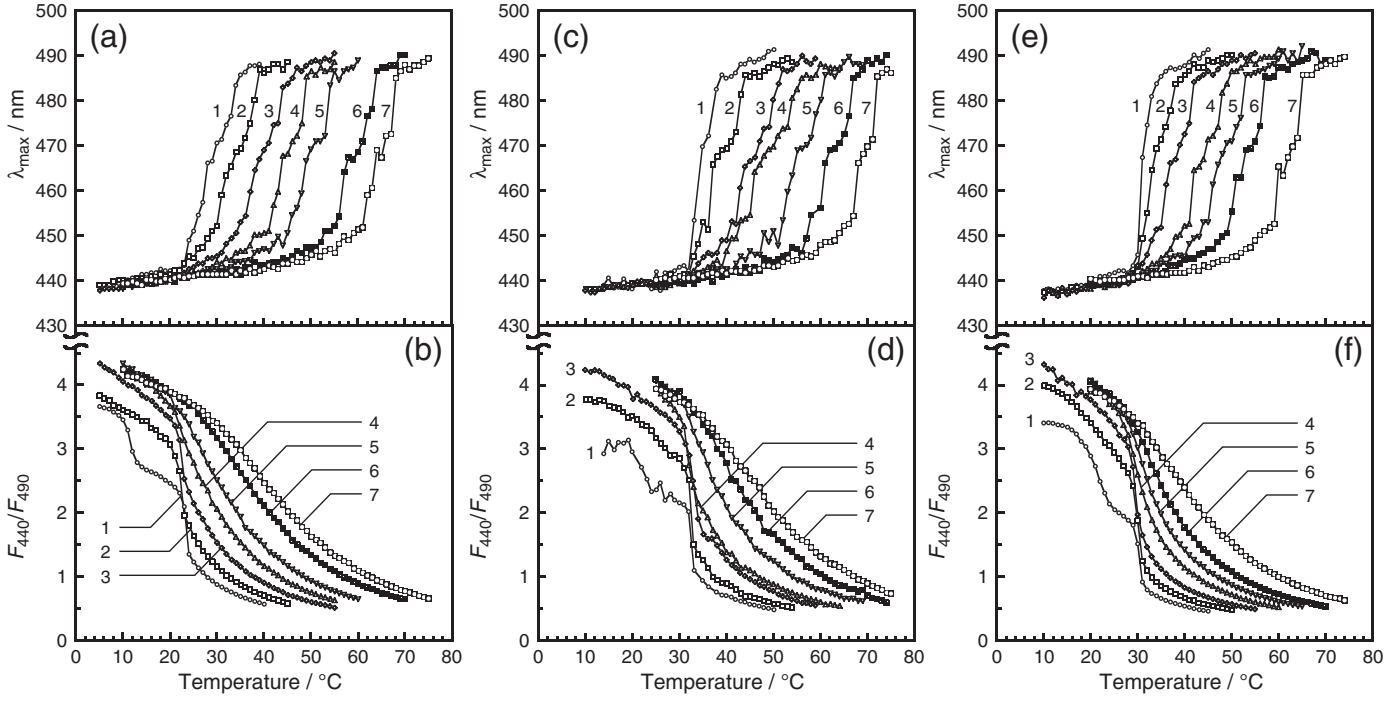

Fig. 3. Temperature dependence of wavelength at the maximum emission (λ_{max}) and ratio of the intensity at 440 nm (F_{440}) to that at 490 nm (F_{490}), i.e., F_{440}/F_{490}, for C14PC–cholesterol ((a) and (b)), C15PC–cholesterol ((c) and (d)) and C16PC–cholesterol ((e) and (f)) binary bilayers at different cholesterol compositions (X_{ch}): (1) $X_{ch} = 0.01$, (2) 0.05, (3) 0.10, (4) 0.14, (5) 0.19, (6) 0.25, (7) 0.31 for C14PC–cholesterol; (1) $X_{ch} = 0.01$, (2) 0.05, (3) 0.10, (4) 0.14, (5) 0.20, (6) 0.25, (7) 0.30 for C15PC–cholesterol; (1) $X_{ch} = 0.01$, (2) 0.05, (3) 0.10, (4) 0.15, (5) 0.19, (6) 0.24, (7) 0.31 for C16PC–cholesterol.

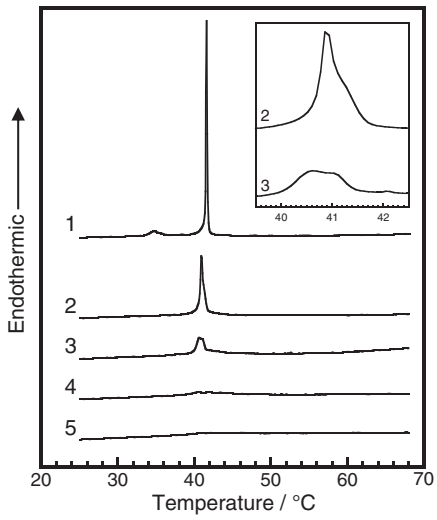

Fig. 4. DSC thermograms of C16PC–cholesterol binary bilayer membranes at different cholesterol compositions (X_{ch}): (1) $X_{ch} = 0$, (2) 0.07, (3) 0.14, (4) 0.20, and (5) 0.30. The magnified views of the endothermic peaks of thermograms 2 and 3 are shown in the inset. Each thermogram is vertically shifted appropriately to avoid overlapping one another.

and only the broad peak apparently remained in the DSC thermogram at higher Chol compositions. This peak corresponds to the higher-temperature peak of the two component peaks and became progressively smaller and markedly broader with further increases in X_{ch}, and finally undetectable at $X_{ch} \geq 0.35$. The C15PC– and the C14PC–Chol binary bilayers exhibited qualitatively similar X_{ch}-dependent behavior of the main transition (shown in Fig. S as supplementary material).

Fig. 5(a)–(c) shows the X_{ch} dependence of the main-transition enthalpy (ΔH_m), the main-transition temperature (T_m) and the peak width at half height of the main transition peak ($\Delta T_{1/2}$), respectively, for all the binary bilayers investigated in this study. As seen from Fig. 5(a), the ΔH_m value decreased almost linearly with increasing X_{ch} and became zero between $X_{ch} = 0.30$ and $X_{ch} = 0.35$ irrespective of the chain length n of the constituent CnPC molecules. It is known that when Chol is incorporated into saturated phospholipid bilayers it suppresses the *trans–gauche* conformational change of the hydrocarbon chains of the constituent phospholipid molecules around it to enhance the conformational order of the hydrocarbon chains above the main-transition temperature [10]. Therefore, the almost linear decrease in ΔH_m with X_{ch} indicates that the population of the phospholipid molecules that have a potential to cause the main transition (i.e., chain-melting transition) decreases nearly in proportion to the amount of Chol incorporated into the bilayer. Further, the fact that ΔH_m becomes zero at least above $X_{ch} = 0.35$ suggests that the thermally induced chain melting no longer occurs in the binary bilayer above that X_{ch} value; that is, that amount of Chol is enough to suppress the *trans–gauche* conformational change of the hydrocarbon chains of all the phospholipid molecules in the binary bilayer.

As shown in Fig. 5(b), T_m decreased slightly with increasing X_{ch} to ca. 0.10 for all the binary bilayers investigated, although a substantial elevation of T_m was observed in the higher X_{ch} region (see the T–X_{ch} phase diagram in the next section). The solid lines shown in Fig. 5(b) represent the X_{ch} dependence of T_m expected from the following thermodynamic relation:

$$\ln(1-X_{ch}) = \frac{\Delta H_m^{\circ}}{R}\left(\frac{1}{T_m} - \frac{1}{T_m^{\circ}}\right) \quad (2)$$

Here, ΔH_m° is the enthalpy change with the main transition of the pure CnPC bilayer, T_m° is the main-transition temperature of the pure CnPC bilayer and R is the gas constant. This equation is based on the simple thermodynamic concept of the liquid–solid phase equilibrium for an ideal binary mixture, and thus inevitably assumes several thermodynamically ideal conditions: (i) in a solid state the two components are perfectly immiscible, (ii) in a liquid state the binary mixture behaves as an ideal dilute solution and (iii) the molar enthalpy of fusion of the solvent in solution is invariant and equal to that of the pure solvent (i.e., ΔH°). Agreements between the experimental and the calculation results were recognized in very dilute X_{ch} regions, namely at most up to 0.02 for the C15PC– and the C16PC–Chol binary bilayers and up to 0.01 for the C14PC–Chol binary bilayer. This can be interpreted as suggesting that the CnPC and the Chol molecules are almost immiscible in the gel ($P_{\beta'}$) phase in

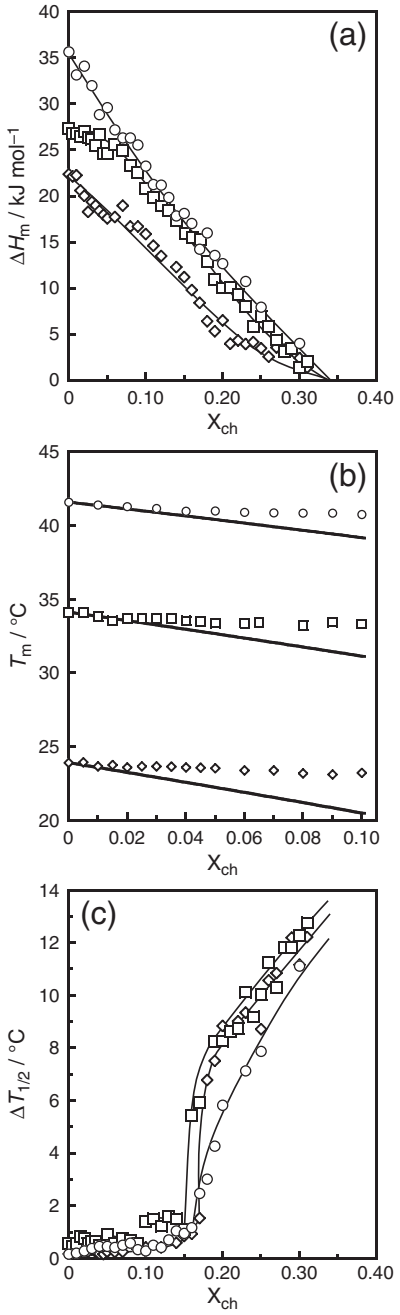

Fig. 5. Cholesterol composition (X_{ch}) dependence of (a) enthalpy change with main transition (ΔH_m), (b) main-transition temperature (T_m) and (c) peak width at half height ($\Delta T_{1/2}$) for C14PC–cholesterol (◊), C15PC–cholesterol (□) and C16PC–cholesterol (○) binary bilayers. In panel (b), solid lines represent the results of the calculation using the general thermodynamic relation of Eq. (2).

those X_{ch} regions because in general the applicability of Eq. (2) tends to be more dependent on the validity of the condition (i) than the others. Above those Chol compositions, the experimental results started to deviate from the calculation curve, which may suggest that Chol becomes partially miscible with C*n*PC within the bilayer even in the $P_{\beta'}$ phase. In the previous studies, we showed that the agreement between the experimental and the calculation results was observed in the X_{ch} region below ca. 0.04 for the C18PC–Chol binary bilayer [23] and below ca. 0.03 for the C17PC–Chol binary bilayer [24]. Taking this into account, the miscibility between Chol and C*n*PC in the gel state is expected to be lower as the acyl chain length of the host C*n*PC molecule increases.

The X_{ch} dependence of $\Delta T_{1/2}$ in Fig. 5(c) suggests that there seems to be a threshold-like Chol composition around $X_{ch} = 0.15$ for all the binary bilayers investigated. The dependence drastically changed around the X_{ch} value: the variation in $\Delta T_{1/2}$ with X_{ch} was relatively small in the X_{ch} region below ca. 0.15, whereas the $\Delta T_{1/2}$ value increased steeply with increasing X_{ch} in the X_{ch} region above ca. 0.15. The remarkable increase in $\Delta T_{1/2}$ in the X_{ch} region above $X_{ch} = 0.15$ is consistent with the results of the Prodan fluorescence measurements; that is, the temperature range where the gradual increase in λ_{max} from 440 nm to 490 nm is observed becomes noticeably wider with increasing X_{ch} in the X_{ch} region above ca 0.15. Therefore, it is reasonable to regard this X_{ch} of ca. 0.15 as a characteristic Chol composition related to some change in the phase behavior of these binary bilayers. Taking into account the fact that the reciprocal of $\Delta T_{1/2}$ is generally related to the cooperativity of the transition, the marked increase in $\Delta T_{1/2}$ observed in the X_{ch} region above ca. 0.15 indicates that the intermolecular cooperation when the chain melting occurs is considerably reduced in this X_{ch} region. Here, we should note that our previous studies [23,24] have revealed that similar X_{ch}-dependent behavior of $\Delta T_{1/2}$ is observed also for the C17PC– and the C18PC–Chol binary bilayers. This means that this characteristic X_{ch} of ca. 015 is common to all the binary bilayers of Chol and C*n*PC (n = 14–18) and independent of the acyl chain length of the host C*n*PC molecule.

Here, we compare the above DSC results with several previous results. The DSC study by McMullen et al. [17] is one of the most systematic studies performed for a homologous series of C*n*PCs (n = 13–21). In the paper, they reported that the pretransition is completely abolished at $X_{ch} > 0.05$ for all the C*n*PC–Chol binary bilayers (n = 14–20). However, in the recent papers by Mannock et al. [32,33], they have noted that later studies using high-sensitivity DSC instruments revealed that the pretransition persists to $X_{ch} = 0.10$ in the C16PC–Chol binary bilayer. Taking this recent result into account, our results about the X_{ch} values of the abolition of the pretransition for the C*n*PC–Chol binary bilayers (n = 14–16) are reasonable. As for the main transition, they have demonstrated that the endothermic peak is composed of a sharp and a broad component and also that the broad component remains until X_{ch} = ca. 0.50 while the sharp component fades out in the X_{ch} range between 0.20 and 0.25. In addition, their results showed that the $\Delta T_{1/2}$ value of the broad component increases steeply with increasing Chol level above X_{ch} = ca. 0.15 for the C14PC– and the C16PC–Chol binary bilayers. Huang et al. [21] have also reported that the main transition of the C16PC–Chol binary bilayer is eliminated at X_{ch} = ca. 0.50 while those of the C18PC– and the C20PC–Chol binary bilayers are not eliminated at the same X_{ch}. Our DSC results are qualitatively consistent with these previous results: the asymmetry of the endothermic peak became noticeable in the intermediate X_{ch} region and the $\Delta T_{1/2}$ value increased steeply with increasing X_{ch} in the X_{ch} region above ca. 0.15. On the other hand, a quantitative agreement was not obtained with respect to the X_{ch} value of the abolition of the main transition. This is thought to be due to the uncertainty in the recognition of the peak. For example, a peak-like variation over a considerably wide temperature range was observed in the DSC thermogram for the C16PC–Chol binary bilayer at $X_{ch} = 0.35$. However, we did not regard it as a peak because the variation was too small in height as compared to the instability of the baseline to define the range of the variation (i.e., the onset and the completion temperature) as a peak. Our decision regarding the peak recognition is supported by the consistency with the results from other techniques. The Prodan fluorescence data obtained in this study indicate that the main transition does not occur at least at $X_{ch} > 0.40$. In addition, several recent studies [34–36] have presented experimental evidence indicating that the pure L_o phase is formed above the $X_{ch} = 0.33$. Especially, the latter evidence is in good agreement with the X_{ch} value of the abolition of the main transition that we estimated from the almost linear relation between ΔH_m and X_{ch} (Fig. 5(a)) as the X_{ch} value at which ΔH_m becomes zero.

3.3. *T*–X_{ch} phase diagrams

Fig. 6(a)–(c) shows possible temperature (T)–X_{ch} phase diagrams of the C14PC–, the C15PC– and the C16PC–Chol binary bilayers constructed on the basis of the above results from the Prodan fluorescence and DSC measurements, respectively. The T–X_{ch} phase diagrams of the C17PC– (Fig. 6(d)) and the C18PC–Chol (Fig. 6(e)) binary bilayers, which have been reported in the previous studies [23,24], are also shown for comparison. We should emphasize here that the phase diagram we presented in this study for each binary bilayer is one of the possible phase diagrams that can successfully explain the experimental results obtained from the Prodan fluorescence and the DSC measurements from the viewpoint of the general thermodynamics of solid–liquid phase equilibria.

The appearance of these phase diagrams resembled a typical solid–liquid phase diagram for a binary mixture which exhibits incongruent melting behavior, and this provides the information about important features of the phase behavior of these binary bilayers. First, it can be inferred from the shapes of the phase boundaries that Chol and these C*n*PCs are, on the whole, immiscible within the bilayers below the eutectic temperature. Note that this never means the perfect immiscibility as assumed in Eq. (2). In fact, a considerable increase in T_m with X_{ch} was observed in the higher X_{ch} region (X_{ch} > ca. 0.25) for each binary bilayer, and as a possible interpretation this increase in T_m is considered to correspond to the solidus line on each phase diagram. In general, solidus and solvus lines are seen in a solid–liquid phase diagram of a binary mixture that can form a homogeneous solid like a solid solution within a limited temperature range, whereas there are no solidus and no solvus lines on the phase diagram of an ideal binary mixture. Therefore, this increase in T_m can be interpreted as a sign of partial miscibility between the phase structures formed in the higher X_{ch} region in the C*n*PC–Chol binary bilayers, although the corresponding solvus line (dashed line in Fig. 6(a)–(c)) could not be experimentally determined in this study. Interestingly, such partial miscibility tends to be less noticeable as the acyl chain of the host C*n*PC molecule increases in length (Fig. 6(d) and (e)).

Another feature of our phase diagrams is that there is a peculiar point like a peritectic point at X_{ch} = ca. 0.15 in each phase diagram. We regarded this point as thermodynamically equivalent to the peritectic point considering that the phase diagrams of a series of C*n*PC–Chol binary bilayers are similar in shape to a typical solid–liquid phase diagram with a peritectic point. A peritectic point occurs as a result of incongruent melting, and this type of melting behavior is usually observed for such binary systems in which the two components react to produce a solid compound with a specific stoichiometry that is stable in a solid state but unstable in a liquid state. The stoichiometry of the solid compound is also reflected in the compositional phase diagram; that is, an isopleth (i.e., a vertical line) always appears at the composition corresponding to the stoichiometry on the phase diagram of such a binary system. Taking this thermodynamic generalization into account, the presence of a peritectic point in our T–X_{ch} phase diagrams of these binary bilayers suggests that a Chol molecule interacts with several C*n*PC molecules within the bilayer to form a complex or a molecular cluster. The stoichiometry of this complex can be presumed to be 1:6 (Chol:C*n*PC, $X_{ch} = 0.143$) independent of the acyl chain length, because the corresponding

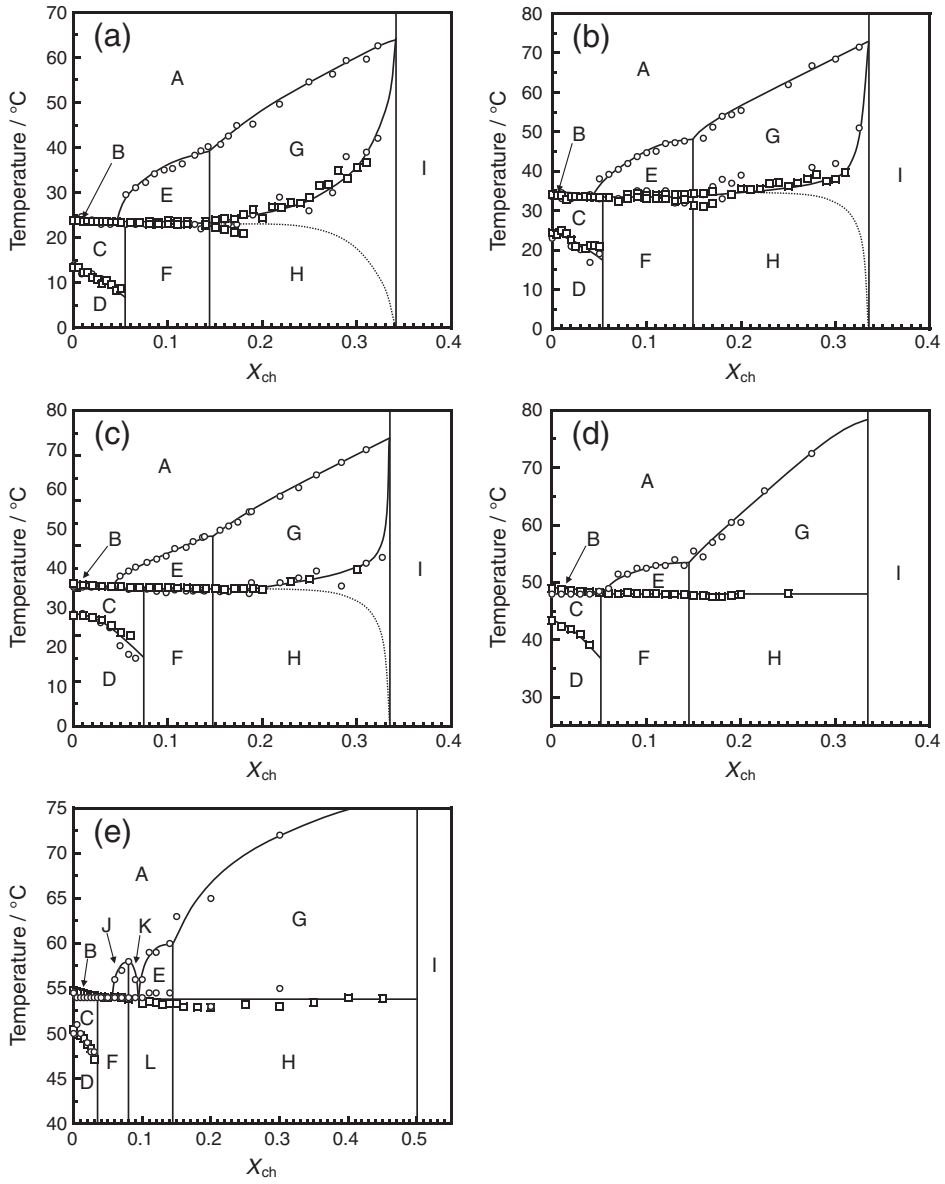

Fig. 6. Temperature (T)–cholesterol composition (X_{ch}) phase diagrams of (a) C14PC–cholesterol, (b) C15PC–cholesterol and (c) C16PC–cholesterol binary bilayers constructed on the basis of the data from Prodan fluorescence (○) and DSC (□) measurements. Our previous results obtained for (d) C17PC–cholesterol [24] and (e) C18PC–cholesterol [23] are also shown for comparison. Phase assignments are as follows: for (a) C14PC–cholesterol, (b) C15PC–cholesterol and (d) C17PC–cholesterol binary bilayer membrane, (A) L_d phase, (B) $L_d + P_{\beta'}$, (C) $P_{\beta'} + L_\beta$ (1:18), (D) $L_{\beta'} + L_\beta$ (1:18), (E) $L_d + L_\beta$ (1:6), (F) L_β (1:18) + L_β (1:6), (G) $L_d + L_o$, and (H) L_β (1:6) + L_o, (I) L_o. For (c) C16PC–cholesterol binary bilayer membrane, the same assignment is applicable by replacing L_β (1:18) with L_β (1:12). For (e) C18PC–cholesterol binary bilayer membrane, the same assignment is applicable except the following: (C) $P_{\beta'} + L_\beta$ (1:30), (D) $L_{\beta'} + L_\beta$ (1:30), (F) L_β (1:30) + L_β (1:12), (J) $L_d + L_\beta$ (1:12), (K) $L_d + L_\beta$ (1:12), and (L) L_β (1:12) + L_β (1:6).

isopleth could be commonly drawn at X_{ch} = ca. 0.15 in our phase diagrams of all the binary bilayers on the basis of the X_{ch} dependence of $\Delta T_{1/2}$ (Fig. 5(c)). As described above, the dependence changed drastically around this X_{ch} value, and we interpreted it as a characteristic composition.

It is also a suggestive feature of our diagrams that two other isopleths are drawn in addition to that at X_{ch} = ca. 0.15. The isopleth at the lowest X_{ch} is relevant to the abolition of the pretransition and the other to the abolition of the main transition. Although these isopleths do not always signify the formation of complexes, the concept of the complex formation is useful to understand the average properties of the binary bilayers in connection with the X_{ch}-dependent phase behavior. In our previous studies on the C17PC–Chol [24] and the C18PC–Chol [23] binary bilayers, we gave a possible explanation for the specific X_{ch} values observed in the phase diagrams based on the so-called *superlattice view*, proposed by Somerharju et al. [25]. According to this view, Chol molecules tend to be distributed regularly within the bilayer and the distribution is well represented using the hexagonal lattice. In fact, experimental evidence indicating the regular distribution of Chol within the binary bilayers has been reported [37–39]. In Fig. 7, schematic illustrations using the hexagonal lattice are given for several types of possible regular distributions of Chol within the binary bilayer. In these illustrations, an open and a closed circle on a lattice point represent a C*n*PC and a Chol molecule, respectively, although in the original superlattice model, either a Chol molecule or an acyl chain of a phospholipid molecule is assigned to a lattice point. We adopted simpler geometry (i.e., one molecule to one site) taking into account the fact that the cross sectional areas of a fully extended hydrocarbon chain, a Chol molecule and a C*n*PC molecule have been roughly estimated at 0.20, 0.40 and 0.55–0.70 nm^2 (depending on X_{ch}) on insoluble monolayers or mixed monolayers, respectively [40–43]. Although these schematic illustrations may give the impression of a rigid and highly ordered membrane, they only explain hypothetical packing states of the binary bilayers presumed as static averaged structures from bulk

thermodynamic properties in terms of the formation of several types of complexes with different stoichiometries.

As shown in Fig. 7(a), when the binary bilayer is entirely occupied with an identical type of fundamental units that are individually composed of a Chol molecule and 18 C*n*PC molecules around a Chol molecule (i.e., Unit (1:18)), the X_{ch} value is equal to 0.053. Similarly, the X_{ch} value is 0.077 for the binary bilayer composed of only Units (1:12), each of which includes a Chol molecule and its surrounding 12 C*n*PC molecules (Fig. 7(b)). The former and the latter X_{ch} values are very close to the experimentally determined X_{ch} values of the abolition of the pretransition for the C14PC– and the C15PC–Chol binary bilayers and for the C16PC–Chol binary bilayer, respectively. The abolition of the pretransition of the C*n*PC bilayer is generally thought to be attributed to the induction of an L_{β}-like phase in the presence of Chol where the orientation of the acyl chains of the C*n*PC molecule is more perpendicular to the bilayer surface [32]. Therefore, this kind of Chol effect can propagate over 18 C*n*PC molecules within Unit (1:18) in the case of C14PC or C15PC and over 12 C*n*PC molecules within Unit (1:12) for C16PC on average. Hereinafter, we use L_{β} (1:18) and L_{β} (1:12) for these states of the binary bilayers, as shown in Fig. 7(a) and (b), respectively.

Two more different types of possible regular distributions of Chol within the binary bilayer are shown in Fig. 7(c) and (d): one is represented by the fundamental unit composed of a Chol molecule and its surrounding 6 C*n*PC molecules (i.e., Unit (1:6)) and the other by Unit (1:2). As apparent from the stoichiometry, the former unit is in accord with the 1:6-complex of Chol and C*n*PCs as discussed above, which means that the formation of the 1:6-complex does not conflict with the superlattice view. In this state, the orientation of the hydrocarbon chains of the C*n*PC molecules is expected to be still perpendicular to the bilayer surface, and thus, we assigned an L_{β} (1:6) phase to this state. We should note that these three types of L_{β} phases are defined as thermodynamically distinct phases in terms of the molecular interaction between Chol and C*n*PC, although they are all gel phases with similar conformational order and molecular orientation. As for Unit (1:2), the X_{ch} value becomes 0.33 when the binary bilayer is occupied entirely with this type of unit. This X_{ch} value is very close to the experimental X_{ch} value for the abolition of the main transition. The abolition of the main transition is generally considered to be due to the complete formation of the L_o phase within the binary bilayer. Taking this into account, the L_o phase is presumed to be a homogeneous state composed by Units (1:2) as illustrated in Fig. 7(d).

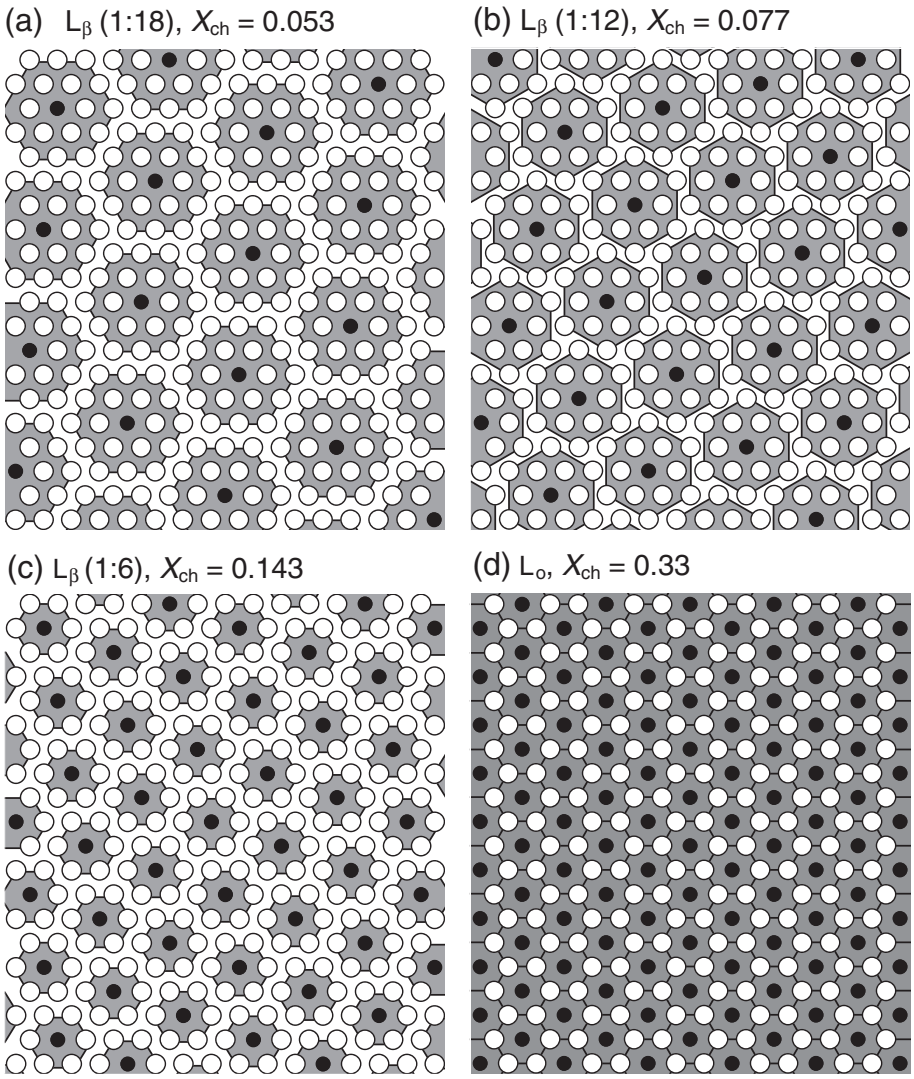

Fig. 7. Schematic illustration for various types of regular distribution of cholesterol in binary bilayer membranes based on hexagonal lattice model. A closed circle and an open circle represent a cholesterol molecule and a C*n*PC molecule, respectively. A fundamental unit is indicated as a dark shaded area around a cholesterol molecule in each panel: (a) L_{β}(1:18) state (X_{ch} = 0.053) composed of only Unit (1:18), (b) L_{β}(1:12) state (X_{ch} = 0.077) composed of only Unit (1:12), (c) L_{β}(1:6) state (X_{ch} = 0.143) composed of only Unit (1:6) and (d) L_o state (X_{ch} = 0.333) composed of only Unit (1:2).

The above explanation regarding the presence of a peritectic point and the complex formation is somewhat speculative, but it is supported by several previous studies. For example, Anderson and McConnell [44] have reported that the formation of complexes containing large numbers of molecules in the phospholipid and Chol binary membrane is rationalized by the thermodynamic calculation based on the extended condensed complex model. It has also been reported in the recent paper by Ariola et al. [45] that the formation of Chol–lipid complexes is indicated by the disagreement between the calculated and the experimental values of the ratio of the translational diffusion coefficient to the rotational diffusion one. Finally, the phase assignments based on the above consideration are summarized as follows. For the T–X_{ch} phase diagrams of the C14PC– and the C15PC–Chol binary bilayers, each area is assigned as follows: A, L_d phase; B, $L_d + P_{\beta}'$; C, $P_{\beta}' + L_{\beta}$ (1:18); D, $L_{\beta}' + L_{\beta}$ (1:18); E, $L_d + L_{\beta}$ (1:6); F, L_{β} (1:18) + L_{β} (1:6); G, $L_d + L_o$; and H, L_{β} (1:6) + L_o; I, L_o. The same assignment is applicable to the T–X_{ch} phase diagram of the C16PC–Chol binary bilayer by replacing L_{β} (1:18) with L_{β} (1:12). It should be noted that the X-ray diffraction study by Karmakar and Raghunathan [46] has shown that the periodically undulated structure (i.e., ripple structure) is formed below the main-transition temperature for the C14PC– and the C16PC–Chol binary bilayers, on the basis of which most of the gel phases observed below the main-transition temperature have been identified as P_{β} or P_{β}' phase. However, such ripple structure can also be formed in the binary bilayers in the L_{β}'–L_{β} coexistence state.

3.4. Chain length dependence of characteristic compositions

On the basis of these phase diagrams of a series of the C*n*PC–Chol binary bilayers (n = 14–18), we consider how the Chol effect on the thermotropic phase behavior is affected by the length of the acyl chains of the host C*n*PC molecules. First of all, we may have to mention the miscibility of Chol and these C*n*PCs. As described above, we found that there is a qualitative tendency that the miscibility of Chol and C*n*PC within the bilayers becomes slightly lower as the acyl chain length increases. This may be attributed to the fact that the van der Waals interaction between the adjacent C*n*PC molecules in the bilayer becomes stronger with increases in the acyl chain length, because two components in a binary mixture tend to be immiscible when the molecular interaction between the same species is stronger than that between different species.

In Fig. 8, we summarized the acyl chain length dependence of the two characteristic X_{ch} values observed in the respective phase diagrams of the C*n*PC–Chol binary bilayers: (A) the X_{ch} at which the main transition is abolished (X_{ch}^{*main}) and (B) the X_{ch} at which the pretransition is abolished (X_{ch}^{*pre}). Our result shows that X_{ch}^{*main} is constant at ca. 0.33 independent of n for n = 14–17, whereas it increases to ca 0.50 at n = 18. Although the X_{ch}^{*main} value of ca. 0.33 is apparently lower than the previous results of McMullen et al. [17] and of Huang et al. [21], our result about the n-dependence of X_{ch}^{*main} shows a tendency similar to those observed in the previous results. First, our result indicating that there is no acyl chain length dependence of X_{ch}^{*main} for n = 14–17 is qualitatively consistent with that of McMullen et al. [17]. Second, the increase in X_{ch}^{*main} at n = 18 observed in this study is similar to the result of Huang et al. [21]. Further, our result about the acyl chain length dependence of X_{ch}^{*main} for n = 14–18 can be explained by the view proposed by McMullen et al. [17]. According to their view, there is no marked dependence on the acyl chain length of the host C*n*PC molecule in the effect of Chol on the thermotropic phase behavior of C*n*PCs with few exceptions, and the exceptions arise chiefly from the mismatch in the effective length of the hydrophobic region between Chol and C*n*PC in the bilayer. Taking into account the fact that this hydrophobic mismatch is minimized at n = 17 [17,32], therefore, the increase in X_{ch}^{*main} to ca. 0.50 at n = 18 can be interpreted as due to the reversal of the hydrophobic mismatch.

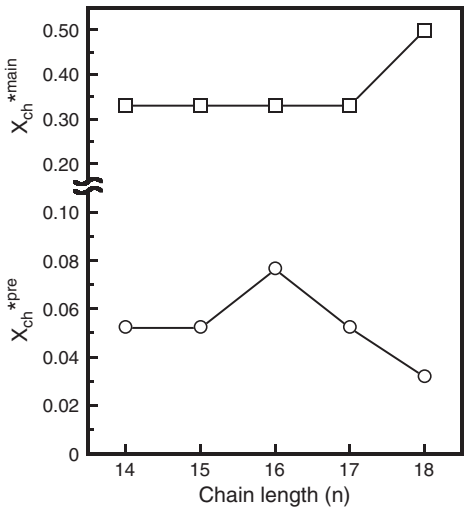

Fig. 8. Acyl chain length (n) dependence of X_{ch}^{*main} (□), i.e., the cholesterol composition at which the main transition is abolished, and of X_{ch}^{*pre} (○), i.e., the cholesterol composition at which the pretransition is abolished.

That is, in the case of C*n*PC with shorter acyl chains ($n \leq 17$), the acyl chains of the C*n*PC molecules around a Chol molecules tend to be forced to be extended to minimize the hydrophobic mismatch, and thus, the incorporation of relatively low composition of Chol can induce the homogeneous L_o phase within the entire binary bilayer. On the other hand, for $n \geq 18$, as has been discussed by Huang et al. [21], the hydrophobic mismatch can create a free volume in the middle of the bilayer which is energetically unfavorable. This could contribute negatively to the complete suppression of the melting of the acyl chains, because the ends of the acyl chains would tend to have a kink to minimize the unfavorable effect of the voids. As a result, relatively large amount of Chol is required to abolish the main transition of the bilayer of C*n*PC with longer acyl chains ($n \geq 18$).

As for X_{ch}^{*pre}, namely the Chol composition at which the pretransition is abolished, a biphasic acyl chain length dependence was observed: X_{ch}^{*pre} increased with an increase in the acyl chain length up to n = 16, whereas it decreased with an increase in the acyl chain length for $n \geq 16$. As described above, the abolition of the pretransition by the incorporation of Chol is thought to be due to the induction of an L_{β}-like orientation. Therefore, the biphasic acyl chain length dependence of X_{ch}^{*pre} suggests that there are at least two antagonistic acyl chain length dependent factors involved in the process of the induction of the L_{β}-like orientation: a factor that accelerates the induction of the L_{β}-like orientation when the acyl chains of the host C*n*PC molecule increase in length and the other one that promotes it when they decrease in length. Currently, we speculate on the induction of the L_{β}-like orientation as follows. Van der Waals interaction is one of the most dominant interaction acting between the neighboring phospholipid molecules in the bilayer and tends to be stronger as the acyl chains becomes longer. The stronger van der Waals interaction is expected to facilitate wider propagation of the Chol effect of inducing the L_{β}-like orientation, and as a result, a smaller amount of Chol is required to induce the L_{β}-like orientation within the entire binary bilayer as the acyl chain length increases: the pretransition is abolished completely at a lower X_{ch} as the acyl chain length increases. Second, we should also take the hydrophobic mismatch into account as an essential factor. In fact, the n value of 16, at which X_{ch}^{*pre} reaches maximum, is very close to that for the minimum hydrophobic mismatch (i.e., n = 17). The bilayer of C*n*PC with shorter acyl chains ($n < 17$) does not have a sufficient thickness of hydrophobic core to accommodate the Chol molecule, and thus, the Chol molecules are expected to be relatively forced out toward the bilayer surface as compared with those in the bilayer of C*n*PC with longer acyl chains ($n \geq 17$). This relative protrusion of the Chol molecule

becomes greater with decreases in the acyl chain length for $n < 17$, which can interfere with repulsive interaction between the adjacent choline headgroups of the host C*n*PC molecules. The weakening of the repulsion will contribute to wider propagation of the Chol effect of inducing the L_{β}-like orientation. As a result, the hydrophobic mismatch for $n < 17$ can also cause the reduction in the amount of Chol needed to induce the L_{β}-like orientation within the entire binary bilayer. This can be the other factor that accelerates the induction of the L_{β}-like orientation as the acyl chain length decreases.

In the last place, we mention that the formation of the 1:6-complex is common to all the C*n*PC–Chol binary bilayers ($n = 14$–18). As seen from the T–X_{ch} phase diagrams, the L_o phase begins to be formed as a phase of two coexisting phases above the X_{ch} corresponding to the 1:6-complex ($X_{ch} = 0.143$). This means that the minimum X_{ch} value for the formation of the L_o phase is independent of the acyl chain length. As far as we know, there have been no reports on how the acyl chain length affects the minimum composition of Chol needed for the formation of the L_o phase. We are now investigating the significance and the meaning of the absence of the acyl chain length dependence for the minimum X_{ch} of the L_o phase formation.

4. Conclusions

In this study, the thermotropic phase transitions of the C*n*PC–Chol binary bilayers ($n = 14$–16) were examined by means of Prodan fluorescence and DSC techniques to construct the T–X_{ch} phase diagrams of these binary bilayers. On the basis of the T–X_{ch} phase diagrams of the C*n*PC–Chol binary bilayers ($n = 14$–16) along with our previous results for the C17PC–Chol [24] and the C18PC–Chol [23] binary bilayers, we found several important features of the thermotropic phase behavior of these binary bilayers. First, the presence of a peculiar point like a peritectic point at X_{ch} = ca. 0.15 was confirmed for all these binary bilayers. This finding indicates that these binary bilayers commonly exhibit not simple eutectic melting behavior but peritectic-like one accompanied with the formation of a 1:6-complex of Chol and C*n*PCs, meaning that the L_o phase begins to be formed at ca. 0.15 regardless of the acyl chain length. Second, in addition to this characteristic X_{ch} of 0.15, two more specific Chol compositions were observed in the phase diagrams: (A) the X_{ch} at which the main transition is abolished ($X_{ch}{}^{*main}$) and (B) the X_{ch} at which the pretransition is abolished (i.e., $X_{ch}{}^{*pre}$). Though these characteristic X_{ch} values were not always constant for the different acyl chain lengths, all the different values of $X_{ch}{}^{*main}$ and $X_{ch}{}^{*pre}$ observed for a series of C*n*PC–Chol binary bilayers ($n = 14$–18) could be explained by different types of regular distributions of Chol within the binary bilayer based on the superlattice view, which can be schematically represented using several possible types of fundamental units, i.e., Unit (1:18), Unit (1:12) and Unit (1:2), on the hexagonal lattice. We could reasonably explain the X_{ch}-dependent peritectic phase behavior of the C*n*PC–Chol binary bilayers on the basis of this concept of the regular distribution.

From the change in the shape of the phase boundaries with the acyl chain length of the host C*n*PC molecules, we found that there is a qualitative tendency that the miscibility of Chol and C*n*PC in the bilayers becomes slightly lower as the acyl chain length increases. This can be explained by the increase in intensity of the van der Waals interaction between the acyl chains of the adjacent C*n*PC molecules in the binary bilayer with increases in the acyl chain length. We also discussed the acyl chain length dependence of $X_{ch}{}^{*main}$ and $X_{ch}{}^{*pre}$. As for $X_{ch}{}^{*main}$, no marked acyl chain length dependence was observed for $n = 14$–17, while $X_{ch}{}^{*main}$ increased to ca. 0.50 in the C18PC–Chol binary bilayer. This increase can be explained by the mismatch in the effective length of the hydrophobic region between the Chol and the C*n*PC molecule. For $X_{ch}{}^{*pre}$, on the other hand, a biphasic acyl chain length dependence was observed: it increased with an increase in the acyl chain length up to $n = 16$, whereas it decreased with an increase in the acyl chain length for $n \geq 16$. This biphasic acyl chain length dependence suggests that there are at least two antagonistic acyl chain length dependent factors involved in the process of the induction of the L_{β}-like orientation. A possible explanation for this is that a wider prevalence of the Chol effect could be brought about by the enhancement of the van der Waals attractive interaction with increases in the acyl chain length and also by the weakening of the repulsive interaction between the neighboring choline headgroups by the presence of Chol with decreases in the acyl chain length for $n < 17$.

Supplementary data to this article can be found online at http://dx.doi.org/10.1016/j.bbamem.2013.06.008.

Acknowledgements

The authors wish to thank the anonymous reviewers for their valuable comments and useful suggestions, which helped to improve this work. A part of this work was supported by JSPS KAKENHI Grant number 24550157.

References

[1] R.N.A.H. Lewis, N. Mak, R.N. McElhaney, A differential scanning calorimetric study of the thermotropic phase behavior of model membranes composed of phosphatidylcholines containing linear saturated fatty acyl chains, Biochemistry 26 (1987) 6118–6126.
[2] H. Ichimori, T. Hata, H. Matsuki, S. Kaneshina, Barotropic phase transitions and pressure-induced interdigitation on bilayer membranes of phospholipids with varying acyl chain-lengths, Biochim. Biophys. Acta 1414 (1998) 165–174.
[3] K. Simons, E. Ikonen, Functional rafts in cell membranes, Nature 387 (1997) 569–572.
[4] L.D. Zajchowski, S.M. Robbins, Lipid rafts and little caves, Eur. J. Biochem. 269 (2002) 737–752.
[5] G.W. Feigenson, J.T. Buboltz, Ternary phase diagram of dipalmitoyl-PC/dilauroyl-PC/cholesterol: nanoscopic domain formation driven by cholesterol, Biophys. J. 80 (2001) 2775–2788.
[6] S.L. Veatch, S.L. Keller, Organization in lipid membranes containing cholesterol, Phys. Rev. Lett. 89 (2002), (268101-1–268101-4).
[7] S.L. Veatch, S.L. Keller, Separation of liquid phases in giant vesicles of ternary mixtures of phospholipids and cholesterol, Biophys. J. 85 (2003) 3074–3083.
[8] B.D. Ladbrooke, R.M. Williams, D. Chapman, Studies on lecithin–cholesterol–water interactions by differential scanning calorimetry and X-ray diffraction, Biochim. Biophys. Acta 150 (1968) 333–340.
[9] R.A. Demel, B. de Kruijff, The function of sterols in membranes, Biochim. Biophys. Acta 457 (1976) 109–132.
[10] P.L. Yeagle, The roles of cholesterol in the biology of cells, in: P.L. Yeagle (Ed.), The Structure of Biological Membrane, second ed., CRC Press, London, 2005, pp. 243–254.
[11] B.R. Lentz, D.A. Barrow, M. Hoechli, Cholesterol–phosphatidylcholine interaction in multilamellar vesicles, Biochemistry 19 (1980) 1943–1954.
[12] D.J. Recktenwald, H.M. McConnell, Phase equilibria in binary mixtures of phosphatidylcholine and cholesterol, Biochemistry 20 (1981) 4505–4510.
[13] J.H. Ipsen, G. Karlström, O.G. Mouritsen, H. Wennerström, M.J. Zuckermann, Phase equilibria in the phosphatidylcholine–cholesterol system, Biochim. Biophys. Acta 905 (1987) 162–172.
[14] M.R. Vist, J.H. Davis, Phase equilibria of cholesterol/dipalmitoylphosphatidylcholine mixtures: ^{2}H nuclear magnetic resonance and differential scanning calorimetry, Biochemistry 29 (1990) 451–464.
[15] P.F.F. Almeida, W.L.C. Vaz, T.E. Thompson, Lateral diffusion in the liquid phases of dimyristoylphosphatidylcholine/cholesterol bilayers: a free volume analysis, Biochemistry 31 (1992) 6739–6747.
[16] J.L. Thewalt, M. Bloom, Phosphatidylcholine: cholesterol phase diagrams, Biophys. J. 63 (1992) 1176–1181.
[17] T.P.W. McMullen, R.N.A.H. Lewis, R.N. McElhaney, Differential calorimetric study of the effect of cholesterol on the thermotropic phase behavior of a homologous series of linear saturated phosphatidylcholine, Biochemistry 32 (1993) 516–522.
[18] T.P.W. McMullen, R.N.A.H. Lewis, R.N. McElhaney, Calorimetric and spectroscopic studies of the effects of cholesterol on the thermotropic phase behavior and organization of a homologous series of linear saturated phosphatidylethanolamine bilayers, Biochim. Biophys. Acta 1416 (1999) 119–134.
[19] T.P.W. McMullen, R.N.A.H. Lewis, R.N. McElhaney, Differential scanning calorimetric and Fourier transform infrared spectroscopic studies of the effects of cholesterol on the thermotropic phase behavior and organization of a homologous series of linear saturated phosphatidylserine bilayer membranes, Biophys. J. 79 (2000) 2056–2065.
[20] T.P.W. McMullen, R.N.A.H. Lewis, R.N. McElhaney, Calorimetric and spectroscopic studies of the effect of cholesterol on the thermotropic phase behavior and organization of a homologous series of linear saturated phosphatidylglycerols, Biochim. Biophys. Acta 1778 (2008) 2814–2822.
[21] T.-H. Huang, C.W.B. Lee, S.K. Das Gupta, A. Blume, R.G. Griffin, A ^{13}C and ^{2}H nuclear magnetic resonance study of phosphatidylcholine/cholesterol interactions: characterization of liquid–gel phases, Biochemistry 32 (1993) 13277–13287.
[22] D. Marsh, Liquid-ordered phases induced by cholesterol: a compendium of binary phase diagrams, Biochim. Biophys. Acta 1978 (2010) 688–699.

[23] N. Tamai, M. Uemura, T. Takeichi, M. Goto, H. Matsuki, S. Kaneshina, A new interpretation of eutectic behavior for distearoylphosphatidylcholine–cholesterol binary bilayer membrane, Biophys. Chem. 135 (2008) 95–101.
[24] N. Tamai, M. Uemura, M. Goto, H. Matsuki, S. Kaneshina, Lateral phase separation in cholesterol/diheptadecanoylphosphatidylcholine binary bilayer membrane, Colloids Surf. B: Biointerfaces 65 (2008) 213–219.
[25] P. Somerharju, J.A. Virtanen, K.H. Cheng, Lateral organisation of lipids: the superlattice view, Biochim. Biophys. Acta 1440 (1999) 32–48.
[26] P.L.G. Chong, Effects of hydrostatic pressure on the location of PRODAN in lipid bilayers and cellular membranes, Biochemistry 27 (1988) 399–404.
[27] M. Kusube, N. Tamai, H. Matsuki, S. Kaneshina, Pressure-induced phase transitions of lipid bilayers observed by fluorescent probes Prodan and Laurdan, Biophys. Chem. 117 (2005) 199–206.
[28] M. Kusube, M. Matsuki, S. Kaneshina, Effect of pressure on the Prodan fluorescence in bilayer membranes of phospholipids with varying acyl chain lengths, Colloids Surf. B: Biointerfaces 42 (2005) 79–88.
[29] M. Goto, H. Sawaguchi, N. Tamai, H. Matsuki, S. Kaneshina, Effect of vesicle size on the Prodan fluorescence in diheptadecanoylphosphatidylcholine bilayer membrane under atmospheric and high pressure, Langmuir 26 (2010) 13377–13384.
[30] M. Goto, T. Matsui, N. Tamai, H. Matsuki, S. Kaneshina, Prodan fluorescence detects the bilayer packing of asymmetric phospholipids, Colloids Surf. B: Biointerfaces 84 (2011) 55–62.
[31] M. Goto, M. Kusube, N. Tamai, H. Matsuki, S. Kaneshina, Effect of hydrostatic pressure on the bilayer phase behavior of symmetric and asymmetric phospholipids with the same total chain length, Biochim. Biophys. Acta 1778 (2008) 1067–1078.
[32] D.A. Mannock, R.N.A.H. Lewis, T.P.W. McMullen, R.N. McElhaney, The effect of variations in phospholipid and sterol structure on the nature of lipid–sterol interactions in lipid bilayer model membranes, Chem. Phys. Lipids 163 (2010) 403–448.
[33] D.A. Mannock, R.N.A.H. Lewis, R.N. McElhaney, Comparative calorimetric and spectroscopic studies of the effects of lanosterol and cholesterol on the thermotropic phase behavior and organization of dipalmitoylphosphatidylcholine bilayer membranes, Biophys. J. 91 (2006) 3327–3340.
[34] C. Yuan, L.J. Johnston, Phase evolution in cholesterol/DPPC monolayers: atomic force microscopy and near field scanning optical microscopy studies, J. Microsc. 205 (2002) 136–146.
[35] J. Zhang, H. Cao, B. Jing, P.F. Almeida, S.L. Regen, Cholesterol–phospholipid association in fluid bilayers: a thermodynamic analysis from nearest-neighbor recognition measurements, Biophys. J. 91 (2006) 1402–1406.
[36] Y. Su, Q. Li, L. Chen, Z. Yu, Condensation effect of cholesterol, stigmasterol, and sitosterol on dipalmitoylphosphatidylcholine in molecular monolayers, Colloids Surf. A Physicochem. Eng. Asp. 293 (2007) 123–129.
[37] P.L.-G. Chong, Evidence for regular distribution of sterols in liquid crystalline phosphatidylcholine bilayers, Proc. Natl. Acad. Sci. U. S. A. 91 (1994) 10069–10073.
[38] D. Tang, B.W. van der Meer, S.-Y.S. Chen, Evidence for a regular distribution of cholesterol in phospholipid bilayers from diphenylhexatriene fluorescence, Biophys. J. 68 (1995) 1944–1951.
[39] J.A. Virtanen, M. Ruonala, M. Vauhkonen, P. Somerharju, Lateral organization of liquid-crystalline cholesterol–dimyristoylphosphatidylcholine bilayers. Evidence for domains with hexagonal and centered rectangular cholesterol superlattices, Biochemistry 34 (1995) 11568–11581.
[40] F. Müller-Landau, D.A. Cadenhead, Molecular packing in steroid–lecithin monolayers, part I: pure films of cholesterol, 3-doxyl-cholestane, 3-doxyl-17-hydroxyl-androstane, tetradecanoic acid and dipalmitoylphosphatidylcholine, Chem. Phys. Lipids 25 (1979) 299–314.
[41] F. Müller-Landau, D.A. Cadenhead, Molecular packing in steroid–lecithin monolayers, part II: mixed films of cholesterol with dipalmitoylphosphatidylcholine and tetradecanoic acid, Chem. Phys. Lipids 25 (1979) 315–328.
[42] I. Brzozowska, Z.A. Figaszewski, Interfacial tension of phosphatidylcholine–cholesterol system in monolayers at the air/water interface, Biophys. Chem. 95 (2002) 173–179.
[43] P. Dynarowicz-Łątka, K. Hąc-Wydro, Interactions between phosphatidylcholines and cholesterol in monolayers at the air/water interface, Colloids Surf. B: Biointerfaces 37 (2004) 21–25.
[44] T.G. Anderson, H.M. McConnell, A thermodynamic model for extended complexes of cholesterol and phospholipid, Biophys. J. 83 (2002) 2039–2052.
[45] F.S. Ariola, Z. Li, C. Cornejo, R. Bittman, A.A. Heikal, Membrane fluidity and lipid order in ternary giant unilamellar vesicles using a new bodipy-cholesterol derivative, Biophys. J. 96 (2009) 2696–2708.
[46] S. Karmakar, V.A. Raghunathan, Structure of phospholipid–cholesterol membranes: an x-ray diffraction study, Phys. Rev. E 71 (2005) 061924.